Applied Science and Biotechnology Journal for Advanced Research e-ISSN: 2583-553X
Peer Reviewed Journal
Volume-2, Issue-5 (September 2023), Page: 9-13 https://doi.org/10.31033/abjar.2.5.3

Preparation of Microwave Induced Ce^{4+} Substitution Properties of Chemically Substituted Zinc Ferrite Nanocrystals

Dr. Arjun Bhosle
Visiting Faculty, Department of Chemistry, Shrikrishna College, Gunjoti, India

Corresponding Author: arjunbhosle401@hotmail.com

Received: 26-08-2023 Revised: 08-09-2023 Accepted: 26-09-2023

ABSTRACT
Sol-gel auto combustion was used to create cerium doped Ni-Cr-Fe spinel ferrite nanoparticles. The cubic spinel structure with co-existence of the CeO2 and Fe2O3 phases is revealed by the XRD patterns of the samples sintered at 600 0C. When Ce4+ ions are added to nickel ferrites, the average lattice constant increases from 8.244 to 8.354 as the crystallite size increases. The well-defined and primarily spherical-shaped grains on the samples' surfaces are visible in SEM micrographs. All of the materials' infrared spectra were captured at room temperature in the 300–800 cm-1 range. The infrared spectra of the current samples also exhibit two major absorption bands, which is a characteristic of spinel ferrites. As the cerium content of Ni-Cr ferrite rises, saturation magnetization (MS) and remnant magnetization (Mr) decline.

Keywords: microwave, substitution properties, chemical, zinc, nanocrystal

I. INTRODUCTION

Spinel ferrites with general chemical formula AB2O4 (where A – is divalent metal ions like Co^{2+}, Mg^{2+}, Zn^{2+}, Ni^{2+}, Mg^{2+} etc. and B – is trivalent metal ion like Fe^{3+}) were discovered in the beginning of 20^{th} century. The name spinel was originated from the Latin word spinella. In the last few decades transition metal ions based ferries with spinel structure have attracted interest of scientist and researchers due to their variety of applications in the field of communication, memory devices, filters, microwave absorbing materials, recording media, core transformers, computer chips etc. [1, 2]. According to crystal structure of spinel ferrite, they can categorize in three categories namely normal spinel, inverse spinel and random spinel. Nickel ferrite is the example of inverse spinel in which divalent metal ions occupies octahedral – B site where as Fe^{3+} ions prefers the tetrahedral – A site. Introduction of rare earth ions in spinel lattice enhances the structural and magnetic properties [3].

Nano-crystalline phase of the ferrite materials shows dramatically changes in their structural, electrical and magnetic properties over the bulk ones. Physical methods of ferrite synthesis such as solid state reaction method have several disadvantages including the addition of secondary impurity phases, difficulty in the formation of uniform crystallites with nano-size etc. In order to obtain the nano-sized ferrite particles with uniform shape and size, chemical methods show good results. Several chemical methods have been adopted for the synthesis of nano-ferrites which includes sol-gel [4], chemical co-precipitation [5], Hydrothermal [6], auto-combustion [7] etc. By the use of chemical co-precipitation method fine particles of nano-ferrites can be obtained, but washing and drying of residual with long time preparation is the difficult task. Since, from the past decade, sol-gel auto-combustion technique becomes extensively used synthesis method with metal nitrates as starting materials and citric acid, glycine and urea as chelating agents.

In the present investigation, nanocrystalline ferrite powders of Ce^{4+} doped nickel ferrites with general chemical formula Ni1-2xCexFeCrO4 were synthesized by using sol-gel auto-combustion technique.

II. SAMPLE SYNTHESIS

Metal nitrates of the constituent ions with chemical formula Ni(No3)2.6H2O, Ce(No3)3.9H2O, Fe(No3)3.9H2O and Cr(No3)3.9H2O were taken as starting materials and citric acid was used as chelating agent. All the metal nitrates were mixed thoroughly in the sufficient amount of distilled water with their weight proportion. Citric acid was taken in the ratio of 1:3 with metal nitrates. The whole mixture was the subjected to continuous stirring at constant temperature of 80^0C on hot plate with magnetic stirrer. At the same time liquid ammonia was slowly added in the mixture to maintain the pH=7. After 2-3 hours of continuous stirring and heating, the solution was converted in viscous sol which was then heated at 150^0C for 20-30 minutes. The sol was then converted into dried gel and suddenly converted into burnt ash after self ignition. The burnt ash was sintered at 600^0C for 6 hours. All the samples were subjected for further study such as structural, morphological and magnetic properties.

III. CHARACTERIZATION TECHNIQUES

All the samples of the series Ni1-2xCexFeCrO4 sintered at 600^0C were characterized by X-ray diffraction technique (XRD), scanning electron microscopy (SEM), infrared spectroscopy (IR) and vibrating sample magnetometry (VSM). Powder X-ray diffraction patterns of all the samples were collected at room temperature on a Philips diffractometer with Cu-K radiations 1.5406 10^{-10} m). All the measurements were taken in the 2□ range of 20^0 to 80^0 with scanning speed of 2^0/min. Infrared spectra of all the samples were recorded at room temperature in the frequency range of 300 cm^{-1} to 800 cm^{-1}. Surface morphology and grain size of the samples was studied by using scanning electron micrographs and transmission electron micrographs. Vibrating sample magnetometer was employed for the measurements of magnetic parameters such as saturation magnetization, remnant magnetization and coercivity etc.

IV. RESULTS AND DISCUSSION

To study the changes in the crystalline structures, the XRD patterns of all the prepared samples are presented in Figure 1 (Left panel). Reflections are observed for the planes (210), (220), (311), (222), (400) (421), (430), (333), (440) and (433) which are related to the cubic spinel structure. The additional peaks confirm the co-existence of CeO2 and □-Fe2O3 phases in the samples. Sample of un-doped Ce ions (x = 0.0) shows the coexistent of □-Fe2O3 (JCPDS card 33-0664) and □-Fe2O3 (JCPDS card 39-1356) phases. It also shows the rhombohedral phase of Cr2O3 (JCPDS card 38-1479). It was found that Cr rich materials show predominantly Cr2O3 and $A^{II/III}$Cr2O4, which is in good agreement with the literature a report [18]. The formation of the Fe2O3– Cr2O3 solid solution is depending on the synthesis conditions and synthesis temperature in particular. Similar results indicating the phases of cerium in XRD are also reported in the literature [24]. The increase in Ce resulted in increase of the rhombohedral crystal structure of -Fe2O3 (JCPDS no. 79-0007).

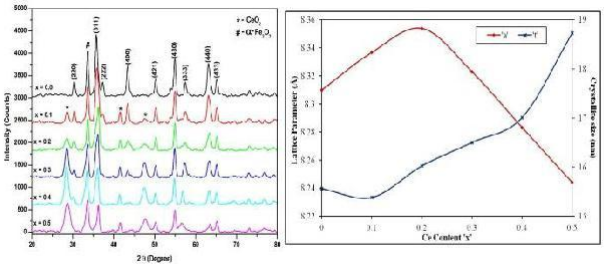

Figure 1: (Left panel) X-ray diffraction patterns of Ni1-2xCexFeCrO4 sintered at 600^0C and (Right panel) variation of lattice parameter ‘a’ and crystallite size ‘t’ with Ce content ‘x’

The lattice constant ‘a’ of all the samples was by taking the average of lattice constant obtained from all peaks. Following relation was used to evaluate the lattice parameter by using the XRD data.

$$d = \frac{a}{\sqrt{h^2 + k^2 + l^2}} \qquad (1)$$

where, ‘d’ is inter-atomic spacing’s form adjacent planes and h, k, l are the miller indices. Variation of lattice parameter with Ce^{4+} substitution is depicted in Figure 1 (right panel). It is observed that, value of lattice constant increases up to x = 0.2 and thereafter it decreases by the addition of Ce^{4+} ions and obtained in the range 8.244 Å to 8.354 Å. Similar behaviour of lattice parameter is found in the literature [1, 3].

Average crystallite size of pure and Ce doped nickel ferrite samples was calculated by using the FWHM values of most intensive peaks in the following Debye-Scherer’s equation [26],

$$t = \frac{(k\lambda)}{(\beta \mathrm{Cos}\theta)} \qquad (2)$$

Where, k is a constant (0.9), is wavelength (1.5405 Å) of incident X-rays, is Bragg’s angle and is the FWHM (Full width at half maxima) of the peak. Right panel of Figure 1, shows the variation of crystallite size ‘t’ with Ce substitution. Crystallite size of the samples is found in the nano-meter scale. It is clearly observed that the crystallite size increases with the addition of Ce ions in nickel ferrite. The increase in crystallite size may be related to the difference in ionic radii of the constituent ions. In the present case Ce^{4+} an ion having higher ionic radii (1.01Å) replaces the Ni^{2+} ions with smaller ionic radii (0.78Å) which increases the crystallite size. This trend of crystallite size is in accordance with the grain size obtained by SEM. The crystallite size varies from 15.57 nm to 18.73 nm for the samples heated at 600^0C.

Figure 2 shows the infrared spectra of all the samples recorded at room temperature in the wavenumber range of 300 cm^{-1} to 800 cm^{-1}. As a common feature of spinel ferrites, infrared spectra of the present samples also show two main absorption bands in his study observed that the high frequency band 1 is related to the intrinsic vibrations of the metal ions with oxygen atoms at tetrahedral site and low frequency band 2 is related to the vibrations at octahedral site. It is observed that the high frequency absorption band 1 observes in the range 542.3 cm^{-1} to 574.1 cm^{-1} and low frequency absorption band 2 is observed in the range 394.2 cm^{-1} to 413.7 cm^{-1}. It is noticed that both 1 and 2 shows their shift towards higher frequency with the addition of Ce^{4+} ions in Ni-ferrite. As nickel ferrite is an example of inverse and often occupies the octahedral – B site. Thus Ce^{4+} ions with larger ionic radii replace the Ni^{2+} ions with smaller ions radii at octahedral site affects the stretching vibrations of Fe^{3+} and O^{2-}.

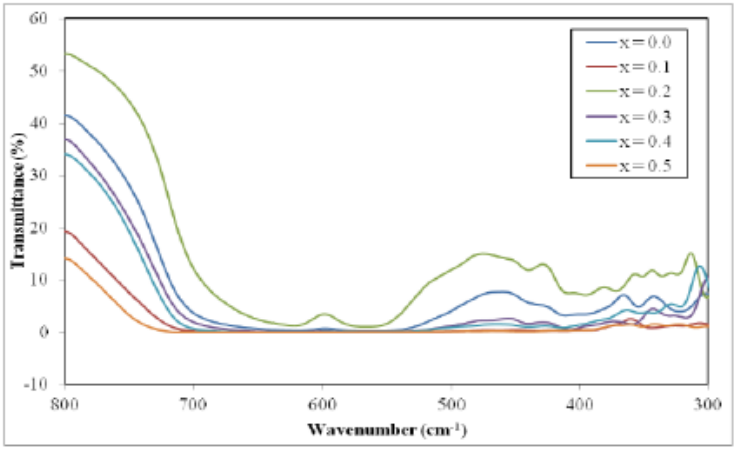

Figure 2: Infrared spectra of Ni1-2xCexFeCrO4

Figure 3 shows the scanning electron micrographs of the end samples (x = 0.0 and 0.5). A keen observation the SEM micrographs shows the well defined and mostly spherical shaped grains on the surface of the samples. The average grain size was estimated for all the samples by using SEM images with the help of online software (Image J). It is observed that average grain size obtained from analysis of SEM images is found in the range 38 to 51 nm. Replacement of Ni ions by Ce ions increases the average grain size which may be attributed due to the larger size of Ce ions. The grain boundary diffusion determines the densification of materials grain boundary migration determines the grain growth. The similar observations are found in previous research for Ce doped Co-Cr and Ni-Zn ferrites.

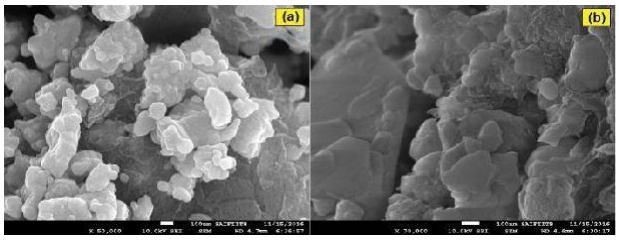

Figure 3: SEM images of $Ni_{1-2x}Ce_xFeCrO_4$ a) x = 0.0 and b) x = 0.5.

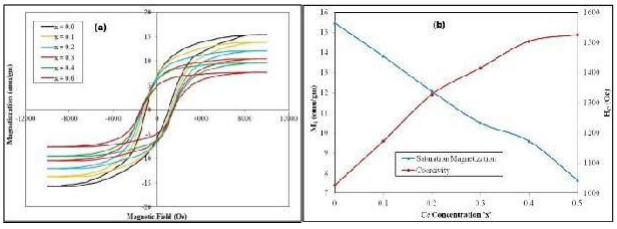

Figure 4: (a) Hysteresis loops of $Ni_{1-2x}Ce_xFeCrO_4$ and (b) variation of saturation magnetization 'Ms' and coercivity 'Hc' with Ce substitution

Figure 4 (a) shows the hysteresis loops of Ce doped Ni-Cr-Fe-O ferrite nanoparticles. The study of these M-H loops gives the information of several magnetic parameters viz. saturation magnetization (MS), remnant magnetization (Mr), coercivity (HC) and squareness ratio (Mr/MS). Introduction of nonmagnetic Ce ions greatly affects on the saturation magnetization of the samples. The variation of saturation magnetization is depicted in Figure 4 (b). Saturation

magnetization (MS) decreases as the cerium percentage in Ni-Cr ferrite increases. This decrease in saturation magnetization with an introduction of Ce ions can be assumed on the basis of following processes,

i. For the selected chemical formula the overall magnetic orientation is reduced.
ii. The magnetic exchange interactions may be weakened after the addition of cerium ions.

Because of the inverse spinel structure of nickel ferrite, Ni^{2+} ions mostly occupy the octahedral – B site and the introduction of cerium ions at octahedral site replaces the Ni^{2+} ions with some Fe^{3+} ions also. Cerium ions have zero magnetic moment which replaces the some Fe^{3+} ions with magnetic moment 5 B. Hence the introduction of nonmagnetic ions dilutes the magnetization at octahedral site which in turn reduces the overall magnetization. Coercivity is related to saturation magnetization (MS) by the relation given by Stoner-Wohlfarth theory,

$$H_C = \frac{0.98 \times K}{M_S} \qquad (3)$$

Figure 4 (b) shows the variation of coercivity (HC) with cerium doped Ni-Cr ferrites. It is found that the coercivity values are lies between the range 1027 (Oe) to 1525 (Oe).

V. CONCLUSIONS

By adopting the sol-gel auto-combustion process, cerium doped Ni-Cr-Fe-O spinel ferrite samples were successfully produced. Each sample has a cubic spinel structure with a geometry in the Fd 3m space group. With the addition of Ce4+ ions, the average crystallite size increased in the spinel lattice. All of the samples' infrared spectra were captured at room temperature, covering the 300 cm-1 to 800 cm-1 wavenumber range. The infrared spectra of the current samples also exhibit two major absorption bands, which is a characteristic of spinel ferrites. The well-defined and primarily spherical-shaped grains on the samples' surfaces are visible in SEM micrographs. The range of average grain size discovered using SEM image analysis is found to be between 38 and 51 nm. The saturation magnetization of the samples is significantly impacted by the introduction of nonmagnetic Ce ions. Saturation magnetization (MS) decreases as the cerium percentage in Ni-Cr ferrite increases.

REFERENCES

1. H. Gul, & E. Pervaiz. (2012). Comparative study of NiFe2-xAlxO4 ferrite nanoparticles synthesized by chemical co-precipitation and sol–gel combustion techniques. *Materials Research Bulletin, 47*, 1353-1361.
2. A. V. Raut, R. S. Barkule, D. R. Shengule, & K. M. Jadhav, (2014). Synthesis, structural investigation and magnetic properties of Zn2þ substituted cobalt ferrite nanoparticles prepared by the sol–gel auto-combustion technique. *J. Magn. Magn. Mater., 358*, 87-92.
3. S. Chakrabarty, M. Pal, & A. Dutta. (2015). Structural, optical and electrical properties of chemically derived nickel substituted zinc ferrite nanocrystals. *Materials Chem. and Phy., 153*, 221-228
4. A. M. M. Farea, S. Kumar, & K. M. Batoo. (2008). Mössbauer studies of Co0.5Cd*x*Fe2.5−*x*O4 (0.0⩽*x*⩽0.5) ferrite. *Physica B: Condensed Matter, 403*(19-20), 3604-3607.
5. H. Gul, A. Z. Abbasi, F. Amin, M. Anis-ur-Rehman, & A. Maqsood. (2007). Structural, magnetic and electrical properties of Co1-xZnxFe2O4 synthesized by co-precipitation method. *J. Magn. Magn. Mater*., *311*, 494–499.
6. H. W. Wang, & S. C. Kung. (2004). Crystallization of nanosized Ni–Zn ferrite powders prepared by hydrothermal method. *J. Magn. Magn. Mater., 270*(1-2), 230-236.
7. A. K. Singh, A. Verma, O. P. Thakur, C. Prakash, T. C. Goel, & R. G. Mendiratta. (2003). Electrical and magnetic properties of Mn–Ni–Zn ferrites processed by citrate precursor method. *Mater. Lett., 57*(5-6), 1040-1044.
8. M. Wahba, & M. B. Mohamed. (2014). Magnetic, and dielectric properties of nanocrystalline Cr-substituted Co0.8Ni0.2Fe2O4 ferrite, *Ceram. Inter., 40*(04), 6127-6135.
9. X. Duan, D. Yuan, Z. Sun, C. Luan, D. Pan, D. Xu, & M. Lv. (2005). Preparation of Co^{2+} doped ZnAl2O4 nanoparticles by citrate sol–gel method, *J. Alloys Compd., 386*(1-2), 311-314.
10. Baykal, N. Kasapoğlu, Y. Köseoğlu, A. C. Başaran, H. Kavas, & M. S. Toprak. (2008). Microwave-induced combustion synthesis and characterization of NixCo1-xFe2O4 nanocrystals (x¼ 0.0, 0.4,0.6,0.8,1.0). *Cent. Eur.J. Chem., 6*, 125-130.
11. M. H. Yousefi, S. Manouchehri, A. Arab, M. Mozaffari, Gh. R. Amiri, & J. Amighian. (2010). Preparation of cobalt–zinc ferrite (Co0.8Zn0.2Fe2O4) nano- powder via combustion method and investigation of its magnetic properties. *Mater. Res. Bull., 45*(12), 1792-1795.
12. G. R. Holcomb, & D. E. Alman. (2006). The effect of manganese addition on the reactive evaporation in Ni-Cr alloys. *Scripta Materialia, 54*(10), 1821-1825.
13. S. E. Shirsath, S. S. Jadhav, B. G. Toksha, S. M. Patange, & K. M. Jadhav. (2011). Influence of Ce^{4+} ions on the structural and magnetic properties of NiFe2O4, *J. Appl. Phys., 110*(01), 013914-18.

14. S. T. Assar, & H. F. Abosheiasha. (2012). Structure and magnetic properties of Co-Ni-Li ferrite synthesized by citrate precursor method. *J. Magn. Magn. Mater.*, *324*(22), 3846-3852.
15. G. Mustafa, M. U. Islam, W. Zhang, Y. Jamil, M. A. Iqbal, M. Hussain, & M. Ahmed. (2015). Temperature dependent structural and magnetic properties of Cerium substituted Co–Cr ferrite prepared by auto-combustion method. *J. Magn. Magn. Mater.*, *378*(15), 409-416.
16. E. Pervaiz, & I. H. Gul. (2013). Low temperature synthesis and enhanced electrical properties of substitution of Al^{3+} and Cr^{3+} in Co-Ni nano ferrites. *J. Magn. Magn. Mater.*, *343*, 194-202.
17. Vivek Choudhari, R. H. Kadam, M. L. Mane, S. E. Shirsath, A. B. Kadam, & D. R. Mane. (2014). Effect of La^{3+} impurity on magnetic and electrical properties of Co-Cu-Cr-Fe nanoparticles, *J. Nanosci. Nanotch.*, *15*(06), 4268-75.
18. R. D. Waldron. (1955). Infrared spectra of ferrites, *Phys. Rev.*, *99*(06), 1727-1735.
19. E. C. Stoner, & E. P. Wohlfarth. (1991). A mechanism of magnetic hysteresis in heterogeneous alloys, *IEEE Trans. Magn.*, *27*(04), 3475-3518.
20. S. H. Liou, S. Hunag, E. Kilmerk, & R. D. Kriby. (1999). Enhancement of coercivity in nanometer – size CoPt crystallites. *J. Appl. Phys.*, *85*(08), 4334-4336.